Brief Report

THROMBOSIS AND HEMOSTASIS

Removal of the vicinal disulfide enhances the platelet-capturing function of von Willebrand factor

Alexander Tischer, Laurie Moon-Tasson, and Matthew Auton

Division of Hematology, Departments of Internal Medicine and Biochemistry and Molecular Biology, Mayo Clinic, Rochester, MN

KEY POINTS

- Removal of the VWF vicinal disulfide bond in A2 enhances platelet adhesion to A1.

- Activation of A1 is a consequence of destabilization-induced domain decoupling.

A redox autoinhibitory mechanism has previously been proposed, in which the reduced state of the vicinal disulfide bond in the von Willebrand factor (VWF) A2 domain allows A2 to bind to A1 and inhibit platelet adhesion to the A1 domain. The VWF A1A2A3 tridomain was expressed with and without the vicinal disulfide in A2 (C1669S/C1670S) via the atomic replacement of sulfur for oxygen to test the relevance of the vicinal disulfide to the physiological platelet function of VWF under shear flow. A comparative study of the shear-dependent platelet translocation dynamics on these tridomain variants reveals that the reduction of the vicinal disulfide moderately increases the platelet-capturing function of A1, an observation counter to the proposed hypothesis. Surface plasmon resonance spectroscopy confirms that C1669S/C1670S slightly increases the affinity of A1A2A3 binding to glycoprotein Ibα (GPIbα). Differential scanning calorimetry and hydrogen-deuterium exchange mass spectrometry demonstrate that reduction of the vicinal disulfide destabilizes the A2 domain, which consequently disrupts interactions between the A1, A2, and A3 domains and enhances the conformational dynamics of A1-domain secondary structures known to regulate the strength of platelet adhesion to VWF. This study clarifies that the reduced state of the A2 vicinal disulfide is not inhibitory but rather slightly activating.

Introduction

The human von Willebrand factor (VWF) mediates platelet adhesion to sites of vascular injury during primary hemostasis.[1,2,3] Proper platelet function of native VWF is dependent on 3 tandem A domains within a C-terminal disulfide-linked dimeric architecture of A, C, and D domains (D′D$_3$-A$_1$-A$_2$-A$_3$-D$_4$-C$_{1-6}$-C$_K$)$_2$ that form long disulfide-linked N-terminal multimers. A1 captures platelets in a shear stress–dependent interaction with platelet receptor glycoprotein Ibα (GPIbα).[4] A2 contains a Y$_{1605}$-M$_{1606}$ scissile bond that is cleaved by the zinc-containing metalloprotease ADAMTS13 to regulate the VWF multimer size.[5] A1 and A3 support VWF adhesion to subendothelial collagen.[6]

A2 also contains a vicinal disulfide bond between C$_{1669}$ and C$_{1670}$ that locks the peptide bond between the cysteines in trans-conformation at the C-terminal α$_6$-Helix, creating a stabilizing hydrophobic interface against the central β-sheet.[5,7] Mutation of this disulfide destabilizes A2 and accelerates proteolysis by ADAMTS13.[8] It has recently been proposed that the redox state of this disulfide regulates the platelet adhesive function of VWF by which the A2 domain, in a reduced state, binds to the sequentially adjacent A1 domain and autoinhibits binding to platelet GPIbα.[1,9]

Recombinant VWF A1A2A3 tridomain (Q$_{1238}$-G$_{1874}$) was expressed in its wild-type form and as cysteine (C$_{1669}$/C$_{1670}$)-to-serine

(Cys→Ser) mutants to test this hypothesis. Cys→Ser represents an atomic replacement of sulfur for oxygen, which is incapable of forming a disulfide linkage. Function, stability, and native-state dynamics of these variants were characterized to assess the impact of these 2 cysteines. These studies show that the loss of the vicinal disulfide enhances GPIbα affinity as well as the shear-dependent platelet adhesion function of A1 by decoupling VWF domain interactions as a mutual consequence of A2 destabilization.

Study design

Wild-type A1A2A3, C1669S/C1670S A1A2A3, wild-type A2, C1669S/C1670S A2, and GPIbα were expressed in HEK293 cells as 6× C-terminally His-tagged fusion proteins. Wild-type A1, wild-type A2, and A2ΔCCS were expressed in Escherichia coli with an N-terminal 6× His-tag. All proteins were purified using nickel-nitriloacetic acid resin, or heparin (wild-type A1 only).[10,11]

Parallel-plate flow-chamber studies were performed with Vena8 GCS biochips (Cellix Bio Ltd) on a Zeiss Axio Observer A1 microscope. Citrated whole blood was perfused over Cu^{2+}-immobilized proteins at shear rates ranging from 800 to 9000 s^{-1}. Videos of translocating platelets were recorded for 60 seconds at 25 frames per second. Tracking analysis was performed as described previously.[11,12]
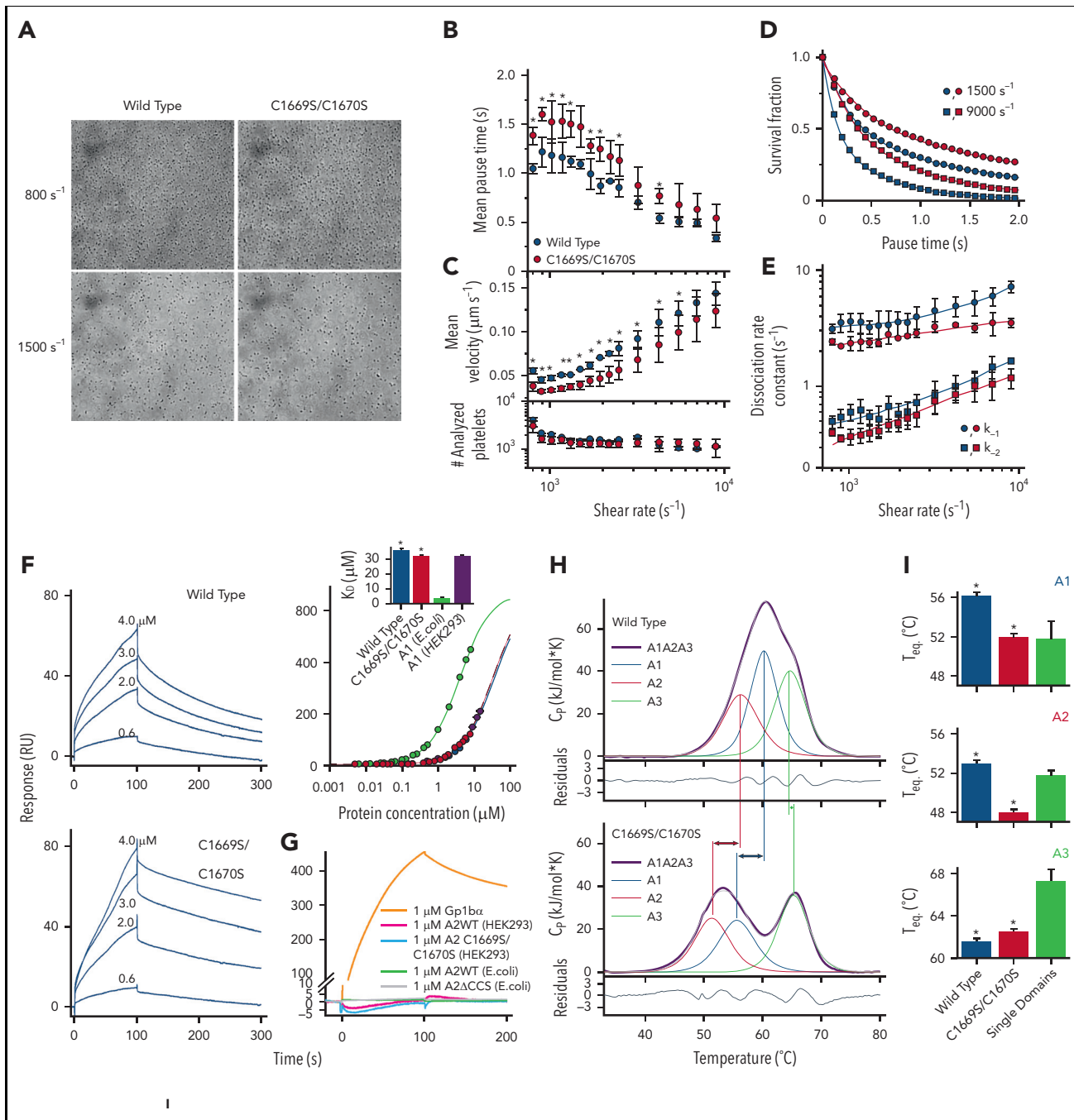
Figure 1. Platelet translocation under shear stress and stability assessment. (A) Representative images of platelets translocating on immobilized wild-type A1A2A3 (left) and C1669S/C1670S A1A2A3 (right) at shear rates of 800 and 1500 s^{-1}. (B) Platelet translocation pause times and (C) translocation velocities and total number of analyzed platelets as a function of shear rate for the wild type (blue symbols) and C1669S/C1670S A1A2A3 (red symbols). Asterisks indicate significance ($P \leq .05$). Only single platelets were tracked in this analysis. (D) Survival fraction decay functions of platelet pause times at 1500 s^{-1} and 9000 s^{-1}. (E) Dissociation rate constants as a function of shear rate obtained from biexponential fitting of the pause time survival fraction decay curves. (F) SPR sensorgrams for both tridomains at concentrations of 4.0, 3.0, 2.0, and 0.6 μM. Comparison of the equilibrium binding curves and GPIbα-binding affinities (inset) for wild-type A1A2A3 and C1669S/C1670S A1A2A3. The resulting apparent K$_D$ values are: 36.1 ± 0.8 μM for wild-type A1A2A3, 32 ± 0.7 μM for C1669S/C1670S A1A2A3; *P* value = .004. Values for A1 either expressed as a single domain in *E coli* (3.9 ± 0.1 μM) or in HEK293 cells (32.4 ± 0.1 μM) were taken from the study by Tischer et al.[13] The global maximum binding signal, RMax, is 670 ± 9 RU. Note that a higher K$_D$-value indicates a lower affinity. (G) Interaction of GPIbα, A2WT (HEK293 or *E coli*), A2 C1669S/C1670S (HEK293), and of A2 ΔCCS (*E coli*) with surface-immobilized wild-type A1 domain. Each protein (1 μM) was perfused over the surface immobilized A1 domain. Although GPIbα binds to the A1 domain, A2 does not interact with A1 regardless of the expression host used, plasmid construct, or the absence/presence of the vicinal disulfide. (H) Thermal denaturation of wild-type and C1669S/C1670S tridomains monitored via DSC (scan rate = 2.0°C/min). Heat capacity thermograms were background corrected relative to the buffer and normalized to a polynomial baseline to define the excess heat capacity. Excess heat capacity was fit using nonlinear least squares analysis and deconvoluted into individual A1, A2, and A3 domain contributions using Wolfram Mathematica per a thermodynamic model in which each domain thermally denatures in a 2-state manner. Both panels contain deconvoluted thermograms of the single domains within the tridomain. Fit residuals are shown at the bottom. Vertical lines and arrows indicate the destabilization of A1 and A2 and a small stabilization of A3 in C1669S/C1670S. (I). Thermal transition temperatures of the deconvoluted domains. A1: 56.2 ± 0.4°C in A1A2A3 vs 51.9 ± 0.4°C in C1669S/C1670S A1A2A3; *P* value ≤ .001. A2: 53.0 ± 0.3°C in A1A2A3 vs 48.0 ± 0.3°C in C1669S/C1670S A1A2A3; *P* value ≤ .001. A3: 61.6 ± 0.3°C in A1A2A3 vs 62.5 ± 0.3°C in C1669S/C1670S A1A2A3; *P* value = .014. T$_{eq.}$ for the single A
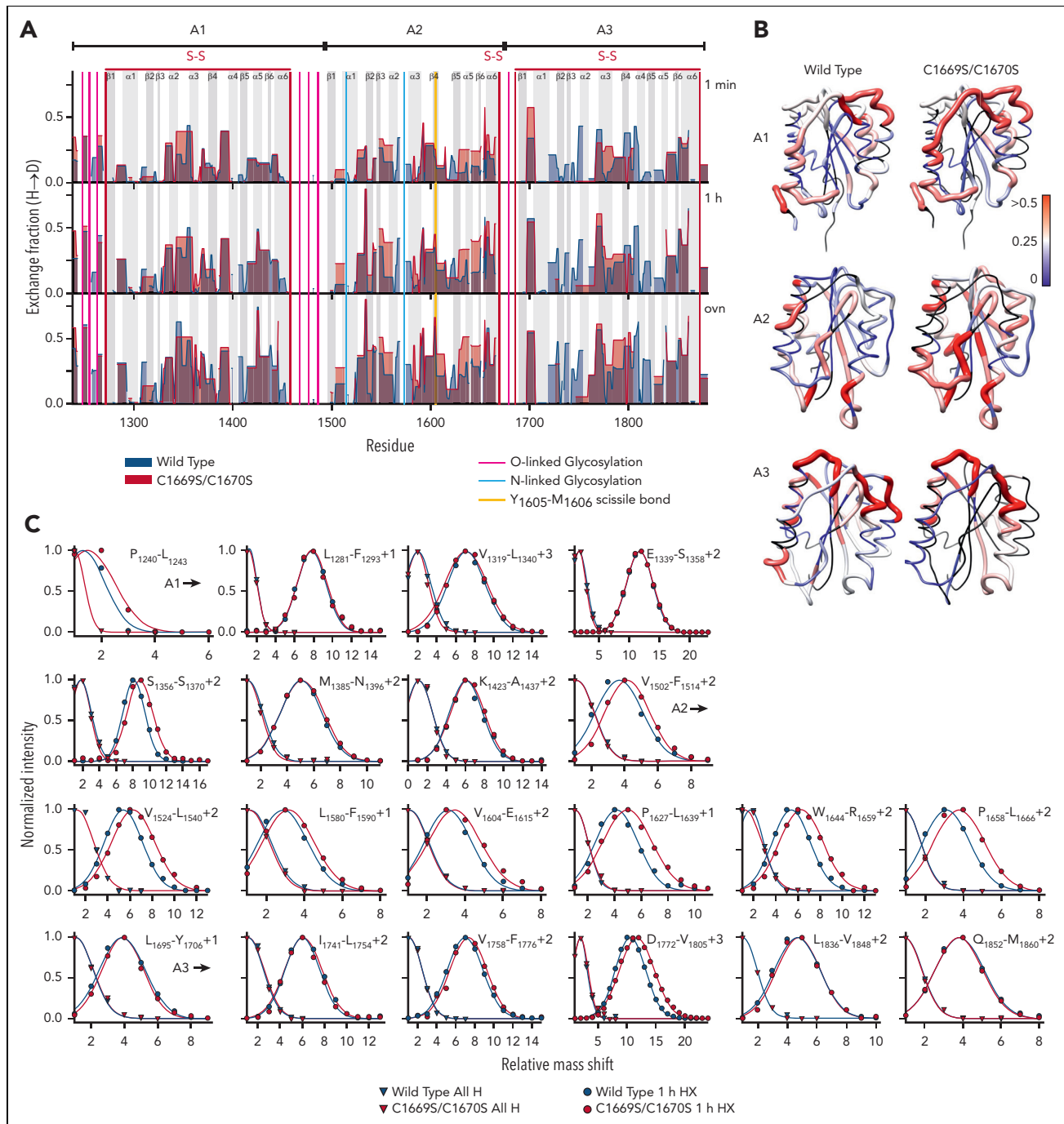
Figure 2. HXMS. Samples were prepared in a 1:5 dilution of A1A2A3 into Tris-buffered saline in deuterium oxide (pD = 7.4). After incubation, hydrogen exchange was quenched by low pD ≅ 2.3. Samples were injected and digested on column with pepsin. Proteolytic fragments were collected on a C_8-trap and separated on a C_{18}-column in line with the mass spectrometer. (A) Hydrogen-deuterium exchange fraction of wild type (blue area) and C1669S/C1670S A1A2A3 (red area) after 1 minute, 1 hour, and 18 hours (top to bottom). (B) One-hour exchange fraction mapped onto the crystal structures of A1 (pdb ID 5BV8),[12] A2 (pdb ID 3gxb),[5] and A3 (pdb ID 1ao3).[6] Black = not resolved, blue = 0, white = 0.25, and red ≥ 0.5. (C) Comparison of peptide envelopes (normalized intensity as a function of the mass shift relative to the "all H" peak) of various peptides within the A1, A2, and A3 domains after 1 hour of exchange. (See supplemental Figures 17-26 for peptide mapping, hydrogen-deuterium exchange fractions as a function of residue number, structural location, time of exchange, and representative peptide envelopes; and supplemental Table 3 for HXMS experimental parameters in the supplemental materials.)

Figure 1 (continued) domains expressed in *E coli*.[12,14,15] A1: 51.8 ± 1.8°C single domain vs 56.2 ± 0.4°C in A1A2A3; *P* value = .014. A2: 51.8 ± 0.4°C single domain vs 53.0 ± 0.3°C A1A2A3; *P* value = .011. A3: 67.2 ± 1.2°C single domain. (See the platelet translocation videos and supplemental Figures 4-7 for an overview of the flow assay and images of translocating platelets at other shear rates; supplemental Figures 8-10 for a comparison of pause time histograms, velocity histograms, and survival fractions at all shear rates; supplemental Table 1 for platelet translocation parameters and statistical analysis using a 2-tailed *t* test; supplemental Figure 11 for SPR response curves of wild-type and C1669S/C1670S A1A2A3 fit to a simple binding model; supplemental Figures 12 and 13 for control experiments for the interactions in *trans* between A2 and A1 and between A2 and GPIbα; supplemental Figure 14 for thermal scan rate dependencies of the excess heat capacity of wild type, C1669S/C1670S, C1669A/C1670A, and C1669G/C1670G that demonstrate that destabilization is independent of the amino acid side chain; supplemental Figure 15 for reproducibility/repeatability of the DSC data; and supplemental Table 2 for DSC parameters in the supplemental materials.)

Differential scanning calorimetry (DSC) was performed on a Nano DSC (TA Instruments). Heat capacity thermograms were background corrected relative to the buffer and normalized to a polynomial baseline to define the excess heat capacity.

Surface plasmon resonance (SPR) was performed on a Biacore T100 using a CM5 chip at 25°C. Anti-FLAG M2 antibody was immobilized, and interactions between A1A2A3 and anti-FLAG–captured GPIbα were determined. Sensorgrams were fit to a simple binding model.[13] To study interactions between wild-type A1 and A2 in *trans*, A1 was immobilized on a CM5 chip surface and interactions with A2 or GPIbα were determined.

Hydrogen-deuterium exchange mass spectrometry (HXMS) was performed using an LTQ Orbitrap XL mass spectrometer and data analysis was performed as previously described.[11]

Results and discussion

Platelet translocation trajectories were analyzed to obtain mean pause times, velocities, and dissociation constants over a range of shear rates, from 800 to 9000 s^{-1}. Figure 1A shows representative platelet adhesion images for the wild type and C1669S/C1670S at 800 s^{-1} and 1500 s^{-1}. Pause times for wild-type A1A2A3 increased to 1.22 ± 0.15 s at 900 s^{-1} and then decreased with increasing shear. C1669S/C1670S has a similar shear dependence, but pause times increased to a maximum of 1.60 ± 0.06 s (Figure 1B). Velocities were decreased for C1669S/C1670S, relative to wild-type A1A2A3, at all shear rates. No differences in platelet coverage were observed (Figure 1C). Pause time survival fractions (Figure 1D) show a biexponential decay, the dissociation rate constants of which are slower for C1669S/C1670S than for the wild type (Figure 1E). SPR demonstrated that the GPIbα-binding affinity of C1669S/C1670S is enhanced compared with that of wild-type A1A2A3 (Figure 1F) and is equivalent to the binding affinity of glycosylated *HEK293*-expressed single A1 domain. Compared with *E coli*–expressed A1, glycosylation in A1A2A3 sterically inhibits binding to GPIbα.[13] SPR also demonstrated that A2, expressed as a separate protein from either *E coli* or HEK293 cells, had no affinity for the A1 domain (Figure 1G).

Deconvolution of the A1A2A3 excess heat capacity traces results in 3 equilibrium transition contributions for each of the domains (Figure 1H). Comparing the transition midpoint temperatures (T$_m$), A2 in C1669S/C1670S A1A2A3 was significantly destabilized relative to the near equivalent T$_m$ of A2 in wild-type A1A2A3 and A2 expressed as a single domain. The T$_m$ of A1 decreased to its intrinsic value as a single domain, indicating that it is stabilized by domain interactions in wild-type A1A2A3. A3 was slightly stabilized toward its intrinsic T$_m$ as a single domain (Figure 1I). C1669S/C1670S uncouples quaternary interactions between A1, A2, and A3. This manifests thermodynamically as 3 domains that unfold independently.

HXMS of A1A2A3 (Figures 2A and B) illustrates that C1669S/C1670S substantially increases local structural dynamics throughout the A2 domain. Peptide envelopes (Figure 2C) confirm that the exchange is globally enhanced throughout the A2 domain. Conversely, A1 and A3 are affected in 3 structural regions: the N-terminus, the α$_2$-loop-α$_3$ region of A1, and the α$_3$-loop-β$_4$ region of A3. These regional dynamics are stabilized by domain interactions in wild-type A1A2A3 and destabilized by C1669S/C1670S. The enhanced dynamics of

the A1 α$_2$-loop-α$_3$-region resulting from type 2B VWD mutations are known play a role in the gain-of-function phenotype.[11,15,16] Overall, hydrogen-exchange dynamics reveal a more flexible domain quaternary structure that exposes the A1 domain, consistent with the thermodynamic observations.

Butera et al concluded that reduced A2 inhibits A1 binding to GPIbα.[1] The present data show that removing the vicinal disulfide within the natural sequence context of A1A2A3 slightly activates A1. The platelet coverage for shear is identical regardless of the presence of a vicinal disulfide. GPIbα equilibrium binding affinity is slightly enhanced, and differences in A1 platelet adhesion activity at all shear rates demonstrate that autoregulation via the vicinal disulfide redox state would not greatly alter the biophysical properties of platelet adhesion.

Interactions between A1 and A2 expressed as separate domains have been described previously.[14,17-19] Molecular dynamics suggests, without confirmation, an interaction between sequentially adjacent A1 and A2 domains.[18,19] Administration of *E coli*–expressed A2 lacking the vicinal cysteines (A2ΔCC) as a separate protein to mice reduced platelet activation and microvesiculation due to traumatic brain injury (TBI).[20] Xu et al claim A2ΔCC prevents a TBI-induced hypercoagulable state of VWF by blocking exposed A1 domains. Our SPR studies (Figure 1G) demonstrate that A2 does not bind to A1 regardless of the presence of the vicinal disulfide. Although A2 cannot capture platelets under shear stress, A2 from *E coli* does bind to GPIbα in solution. This provides an alternative explanation for the protective effect that *E coli*–expressed A2 may have against TBI (see supplemental Figures 12 and 13, available on the *Blood* website).

This comparative study demonstrates that the removal of the A2 vicinal disulfide bond, decouples quaternary interactions between the A1, A2, and A3 domains, exposes A1 secondary structures known to regulate platelet adhesion, and increases A1-GPIbα binding affinity. Loss of domain interactions are consequential to A2 destabilization, which enhances the platelet function of A1. Although this study is limited to the recombinant VWA domains, we expect that their intrinsic properties are correlative to those of the in vivo multimeric species of VWF.[4,11,12] Based on these results, it may be postulated that if the redox state of the vicinal disulfide does fluctuate in vivo, A2 destabilization could enhance VWF proteolytic susceptibility to ADAMTS13.[8] Exposing A1 subsequent to A2 cleavage might contribute to a hypercoagulable state of VWF.[20]

Authorship

Contribution: A.T. performed experiments, analyzed data, and wrote the manuscript; L.M.-T. contributed to the expression of the proteins; and M.A. designed the research, analyzed data, and wrote the manuscript.

Conflict-of-interest disclosure: The authors declare no competing financial interests.

ORCID profiles: A.T., 0000-0001-9909-5262; M.A., 0000-0002-4446-6932.

Correspondence: Matthew Auton, Division of Hematology, Mayo Clinic, 150 3rd Street SW, 6-56 Stabile Bldg., Rochester, MN 55905; email: auton.matthew@mayo.edu.

Footnotes

REFERENCES

1. Butera D, Passam F, Ju L, et al. Autoregulation of von Willebrand factor function by a disulfide bond switch. *Sci Adv.* 2018;4(2):1-12.

2. Sadler JE. Biochemistry and genetics of von Willebrand factor. *Annu Rev Biochem.* 1998; 67:395-424.

3. Springer TA. von Willebrand factor, Jedi knight of the bloodstream. *Blood.* 2014; 124(9):1412-1425.

4. Tischer A, Madde P, Moon-Tasson L, Auton M. Misfolding of vWF to pathologically disordered conformations impacts the severity of von Willebrand disease. *Biophys J.* 2014;107(5):1185-1195.

5. Zhang Q, Zhou YF, Zhang CZ, Zhang X, Lu C, Springer TA. Structural specializations of A2, a force-sensing domain in the ultralarge vascular protein von Willebrand factor. *Proc Natl Acad Sci U S A.* 2009;106(23):9226-9231.

6. Bienkowska J, Cruz MA, Atiemo A, Handin R, Liddington R. The von Willebrand factor A3 domain does not contain a metal ion-dependent adhesion site motif. *J Biol Chem.* 1997;272(40):25162-25167.

7. Richardson JS, Videau LL, Williams CJ, Richardson DC. Broad analysis of vicinal disulfides: occurrences, conformations with cis or with trans peptides, and functional roles including sugar binding. *J Mol Biol.* 2017; 429(9):1321-1335.

8. Luken BM, Winn LY, Emsley J, Lane DA, Crawley JT. The importance of vicinal cysteines, C1669 and C1670, for von Willebrand factor A2 domain function. *Blood.* 2010;115(23):4910-4913.

9. Deng W, Voos KM, Li R. A new redox switch regulating von Willebrand factor activity. *J Thromb Haemost.* 2018;16(7):1257-1258.

10. Auton M, Cruz MA, Moake J. Conformational stability and domain unfolding of the von willebrand factor a domains. *J Mol Biol.* 2007; 366(3):986-1000.

11. Tischer A, Machha VR, Frontroth JP, et al. Enhanced local disorder in a clinically elusive von willebrand factor provokes high-affinity platelet clumping. *J Mol Biol.* 2017;429(14): 2161-2177.

12. Tischer A, Campbell JC, Machha VR, et al. Mutational constraints on local unfolding inhibit the rheological adaptation of von willebrand factor. *J Biol Chem.* 2016;291(8): 3848-3859.

13. Tischer A, Machha VR, Moon-Tasson L, Benson LM, Auton M. Glycosylation sterically inhibits platelet adhesion to von Willebrand factor without altering intrinsic conformational dynamics. *J Thromb Haemost.* 2020;18(1):79-90.

14. Valladolid C, Martinez-Vargas M, Sekhar N, et al. Modulating the rate of fibrin formation and clot structure attenuates microvascular thrombosis in systemic inflammation. *Blood Adv.* 2020;4(7):1340-1349.

15. Tischer A, Machha VR, Rösgen J, Auton M. "Cooperative collapse" of the denatured state revealed through Clausius-Clapeyron analysis of protein denaturation phase diagrams. *Biopolymers.* 2018;109(8):e23106.

16. Zimmermann MT, Tischer A, Whitten ST, Auton M. Structural origins of misfolding propensity in the platelet adhesive von Willebrand factor A1 domain. *Biophys J.* 2015;109(2):398-406.

17. Martin C, Morales LD, Cruz MA. Purified A2 domain of von Willebrand factor binds to the active conformation of von Willebrand factor and blocks the interaction with platelet glycoprotein Ibα. *J Thromb Haemost.* 2007; 5(7):1363-1370.

18. Aponte-Santamaria C, Huck V, Posch S, et al. Force-sensitive autoinhibition of the von Willebrand factor is mediated by interdomain interactions. *Biophys J.* 2015;108(9): 2112-2321.

19. Posch S, Aponte-Santamaria C, Schwarzl R, et al. Mutual A domain interactions in the force sensing protein von Willebrand factor. *J Struct Biol.* 2017;197(1):57-64.

20. Xu X, Wang C, Wu Y, et al. Conformation-dependent blockage of activated VWF improves outcomes of traumatic brain injury in mice. *Blood.* 2021;137(4):544-555.